SIAM J. APPL. MATH.
Vol. 63, No. 1, pp. 195–221

HYDRODYNAMIC CLEANSING OF PULMONARY ALVEOLI*

DAPHNE ZELIG† AND SHIMON HABER‡

Abstract. The inside wall of the pulmonary alveolus is lined with a thin viscous fluid layer and a monolayer of surfactants. Inhaled foreign particles that reach the lung alveoli are normally neutralized by macrophages and remain inside the lung. Nevertheless, Podgorski and Gradon [*Ann. Occup. Hyg.*, 37 (1993), pp. 347–365] suggested that a hydrodynamic cleansing mechanism may exist in which particles are swept out by the net fluid flow from the alveolar viscous layer to the adjacent airways. Hawgood [*The Lung: Scientific Foundations*, 2nd ed., R. G. Crystal and J. B. West, eds., Lippincott-Raven, Philadelphia, 1997, pp. 557–571] has also reported that surfactants exit the alveoli during every breathing period. Based upon the foregoing observations, we examine a possible mechanism of hydrodynamic cleansing and predict its effectiveness. Our central assumption is that the amount of surfactant remains periodic during breathing and that a certain regulatory mechanism exists that causes excess surfactant (reported by Hawgood) to leave the alveoli. Owing to the latter, surfactant concentration gradients are induced inside the alveoli, which in turn generate fluid motion (a Marangoni effect) and concomitant fluid discharge. Our analysis predicts that a typical value of the outflow velocity is 10^{-9}[m/sec]; i.e., it takes a fluid particle almost two days to travel a distance equal to an alveolar radius. It is also shown that the outflow velocity depends almost linearly on the discharge rate of the surfactants. Hence, a small artificial addition of surfactants into the lung may enhance alveolar cleansing, provided that a biological mechanism exists that maintains normal surfactant concentration over the lining fluid layer.

Key words. lung alveoli, hydrodynamic cleansing, surfactants

AMS subject classifications. 76Z05, 92C35

PII. S0036139901386090

1. Introduction.

Zeltner et al. [29] observed that a nonuniform pattern of particle deposition exists within the rodent lung. Specifically, the density of particles deposited on the alveolar entrance rim is five times higher than that on septal alveolar surfaces. Are hydrodynamic forces driving the particles from their initial deposition locations toward the entrance rim? The fluid dynamical problem addressed in this paper is motivated by the search for such a possible cleansing mechanism inside the lung alveoli.

Environmental and occupational hazards resulting from aerosol inhalation have been the subject of intensive research (see Harvey and Crystal [14]). An understanding of aerosol kinetics may also prove to be a meaningful step towards improving diagnostic and therapeutic methods [1], [5]. In humans, the respiratory airway system consists of the nasal cavity, the throat, the voice box, the trachea, the two primary bronchi that bifurcate from the trachea, the bronchi, and bronchiole that divide and subdivide, becoming steadily smaller until there are about 20–23 generations of branching. From the sixteenth generation, the airways become increasingly alveolated. The bronchioles terminate with berry-shaped group of sacs and acinar ducts (the acinus). During breathing, the alveoli and the alveolar ducts expand and contract in a way roughly consistent with geometric similarity. Thus, all dimensions scale approximately as the 1/3 power of the lung volume (Gil and Weibel [8], Gil et al. [7]; Weibel [27]; Ardila,

*Received by the editors March 7, 2001; accepted for publication (in revised form) April 2, 2002; published electronically August 28, 2002.
http://www.siam.org/journals/siap/63-1/38609.html
†Department of Mathematics, Technion, Israel Institute of Technology, Haifa 32000, Israel (motiz@012.net.il).
‡Department of Mechanical Engineering, Technion, Israel Institute of Technology, Haifa 32000, Israel (mersh01@tx.technion.ac.).

Horie, and Hildebrandt [2]). Tsuda, Henry, and Butler [25], Tsuda, Otani, and Butler [26], and recently Haber et al. [12] considered the effect of alveolar expansion and contraction on the fluid flow inside the alveoli. In [25] and [26], the authors assumed that the pulmonary acinus could be viewed as a self-similar expanding axisymmetric thoroughfare surrounded by a toroidal sac, a configuration that simplified the numerical calculations. In [12], the alveolus was geometrically approximated by a self-similar expanding spherical cap attached at its rim to the alveolar duct (see also Gil et al. [7]), a geometry that is likely to represent a more faithful portrayal of the acinus.

Little attention has been paid in the past to the effect of alveolar expansion and contraction, since in the case of gas exchange the Peclet number controlling the transport of the gas molecules is much smaller than unity. Thus, convection due to the acinar flow is negligibly small when compared with the diffusive transport. (It takes only a few milliseconds for a gas molecule to reach the alveolar wall from its entrance ring.) However, in the case of aerosol transport, the Peclet number is much larger, and particle convection and diffusion may play a comparable role. Under normal conditions, particles 0.5 to 4 μm in diameter may often reach the acinus and pose the greatest hazard to human health (see, e.g., Dockery et al. [6]).

Particles that enter the respiratory system and are deposited over the airway walls are mechanically removed by the rhythmical motion of cilia (Sleigh, Blake, and Liron [20]). Particles are forced upwards along the bronchiolar tree and are finally removed from the respiratory system by forced convection of air (coughing). Nonetheless, a similar cleansing mechanism does not exist within the acinus. Generally, particles that reach the alveoli are neutralized by macrophages [4] and remain deposited inside the acinus. Indeed, several experimental studies (e.g., Zeltner et al. [29], Heyder et al. [16], Schultz et al. [24]) have investigated such aerosol mixing and deposition. However, Gradon and Podgorski [11] proposed that a purely hydrodynamic effect may assist in cleansing the alveoli. They suggested that gradients in surfactant concentrations induce the thin fluid lining that covers the inner alveolar wall to flow slowly outside the alveolus rim. Thus, particles deposited on the alveolar wall are carried with the fluid toward the entrance rim. They predicted a characteristic clearance time of about one hour.

Scarpelli [23] described the main stages of the surfactant's transition between the air-fluid interface and the fluid body as follows: During expiration, the alveolus contracts and the distance between the surfactant molecules decreases; in other words, their concentration increases and consequently the surface tension diminishes. When the alveolar radius reaches a threshold value, some of the molecules of the surfactant leave the interface and penetrate the fluid. During inspiration, the alveolus expands, the concentration of the surfactant decreases, and concomitantly, the surface tension increases. In addition, surfactants return to the interface from the bulk of the fluid by diffusion. More detailed models for surfactant transition can be found in [9], [10].

In [15], the metabolism of surfactants is explained, and the secretion rate is evaluated. There is clear evidence for the existence of a regulatory mechanism for surfactant production and clearance rates that keeps it from excessive accumulation or dilution [15]. Surfactants are created in Type II cells, which form part of the alveolus wall. After diffusing to the interface, most of them (about 80%) return to these cells and are then recycled for additional use. About 10–20% are consumed by macrophages, which lie at the alveolar wall, and the remaining few percent exit the alveolus.

In this article the alveolar hydrodynamic clearance mechanism is analyzed. We adopt the spherical model that has been extensively used in the past (e.g., Podgorski

and Gradon [22] and Haber et al. [12]) to describe the alveolus configuration. We also use measured experimental data for alveoli expansion/contraction rates and the known measured correlation between surfactant concentration and surface tension. We focus on the dynamical behavior of the surfactants, the main mechanism that controls the lining fluid flow, and assume that no surfactants are accumulated or depleted inside the alveolus during a breathing cycle. The boundary condition at the alveolar rim is based upon the known experimental value of the small amount of surfactant exiting the alveolus per breathing cycle. An open and valid question is what the specific mechanism that causes surfactant to exit the alveolus might be. One might assume, for instance, that airflow in the adjacent airway contributes to the sweeping effect, and reformulate the boundary conditions accordingly. Another possibility is that there is a biological mechanism that discharges excess surfactant from inside the alveolus. We try to avoid such ad hoc assumptions and focus on a cleansing mechanism that is based upon known and validated experimental data. The solution methodology is based on the assumption that, had no fluid been driven through the alveolus opening, surfactant concentration would have been uniform and the lining fluid would have expanded and contracted in a radially symmetric manner to conserve fluid mass. Thus, scaling of the cleansing mechanism is based upon the amount of surfactant leaving the alveolus, a markedly different approach from that used by Podgorski and Gradon [22], who relate the continuity of the fluid and the surfactant layers at the alveolar rim. A source term is also added to the surfactant mass conservation equation to account for surfactants entering or leaving the interface from the bulk fluid, and this facilitates the condition that no mass accumulation or depletion of surfactants per cycle occurs. As a result, the whole set of equations and the solution differ markedly from that obtained by Podgorski and Gradon [22].

In section 2, we define the geometrical, kinematical, and physiological parameters that scale the variables of the problem. In section 3, we obtain the resulting governing equations, boundary conditions, and parameters that control the problem. In section 4, we present the asymptotic expansion of the flow variables in terms of two smallness parameters and obtain the equations and boundary conditions that govern the zero and first order approximations. In section 5.1, we present the analytic solution of the zero order approximation, and in section 5.2, a finite element analysis is utilized to obtain a solution for the first order approximation. In section 6, we discuss our results, and we present our concluding remarks in section 7.

2. The alveolus model: Configuration and typical parameters. Assume that the alveolus can be approximated by a hollow spherical cap of radius $R(t)$ attached at its rim to the alveolar duct (see Figure 1). Typical alveolar mean radius ranges between 40 and 200μm. The alveolus is rhythmically expanding and contracting with a breathing rate of 12–14 breaths per minute for adults and about 33 breaths per minute for infants. The expansion amplitude is about 0.1 alveolar radius. The dependence of R on time is based on experimental data described in Podgorski and Gradon [22] and approximated here by a natural cubic spline interpolation to achieve continuity of its time derivatives (see Figure 2(a)).

A spherical coordinate system (r, θ, ϕ) is located at the center of the spherical cap, where r stands for the radial coordinate and θ and ϕ denote the latitude and azimuthal angles, respectively.

The alveolus rim location is defined by the half-cone angle θ_b. (Henceforth, we assume that $\theta_b = 60^0$ and that the subscript "b" denotes evaluation at the rim.) The inside wall of the alveolus is lined with a thin fluid layer of thickness $h(\theta, \phi, t)$. The

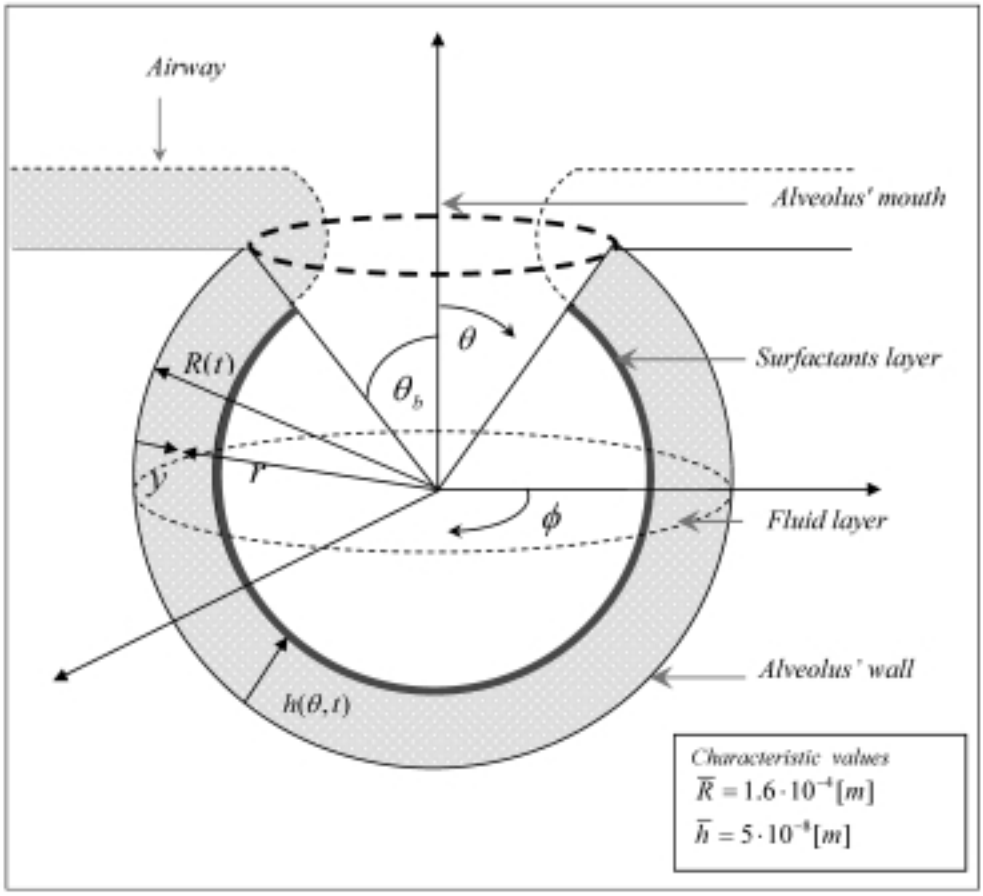

FIG. 1. *A schematic description of the alveolus.*

fluid layer is lined with a single layer of surfactant that lies at the fluid-air interface.

During expansion, additional surfactants are produced at the alveolus wall and diffuse through the fluid bulk into the fluid-air interface. Most of these retract to the fluid layer when the alveolus contracts. A residual part is cleared through the alveolar rim at $\theta = \theta_b$. Thus, a useful partition of the total rate of surfactant production $F(t)$ is

$$F(t) = \frac{\overline{m}(\lambda_b F_b(t) + \lambda_{ec} F_{ec}(t))}{T},$$

where T stands for the breathing period and $\overline{m}$ is the time-averaged amount of surfactants found in the alveolus. (Henceforth, the overhead-bar sign denotes either an average or a typical value.) The first term $\overline{m}\lambda_b F_b(t)/T$ is the rate of production of surfactants that are cleared from the alveolus rim at $\theta = \theta_b$. The prefactor $\overline{m}\lambda_b/T$ is used to scale the production rate so that the time dependent function $F_b(t)$ is of order unity.

The second term $\lambda_{ec}\overline{m}F_{ec}(t)/T$ is a periodic function with zero mean that stands for the rate of transit of surfactant between the fluid bulk and the air-fluid interface during the expansion and contraction process. The prefactor $\lambda_{ec}\overline{m}/T$ scales its

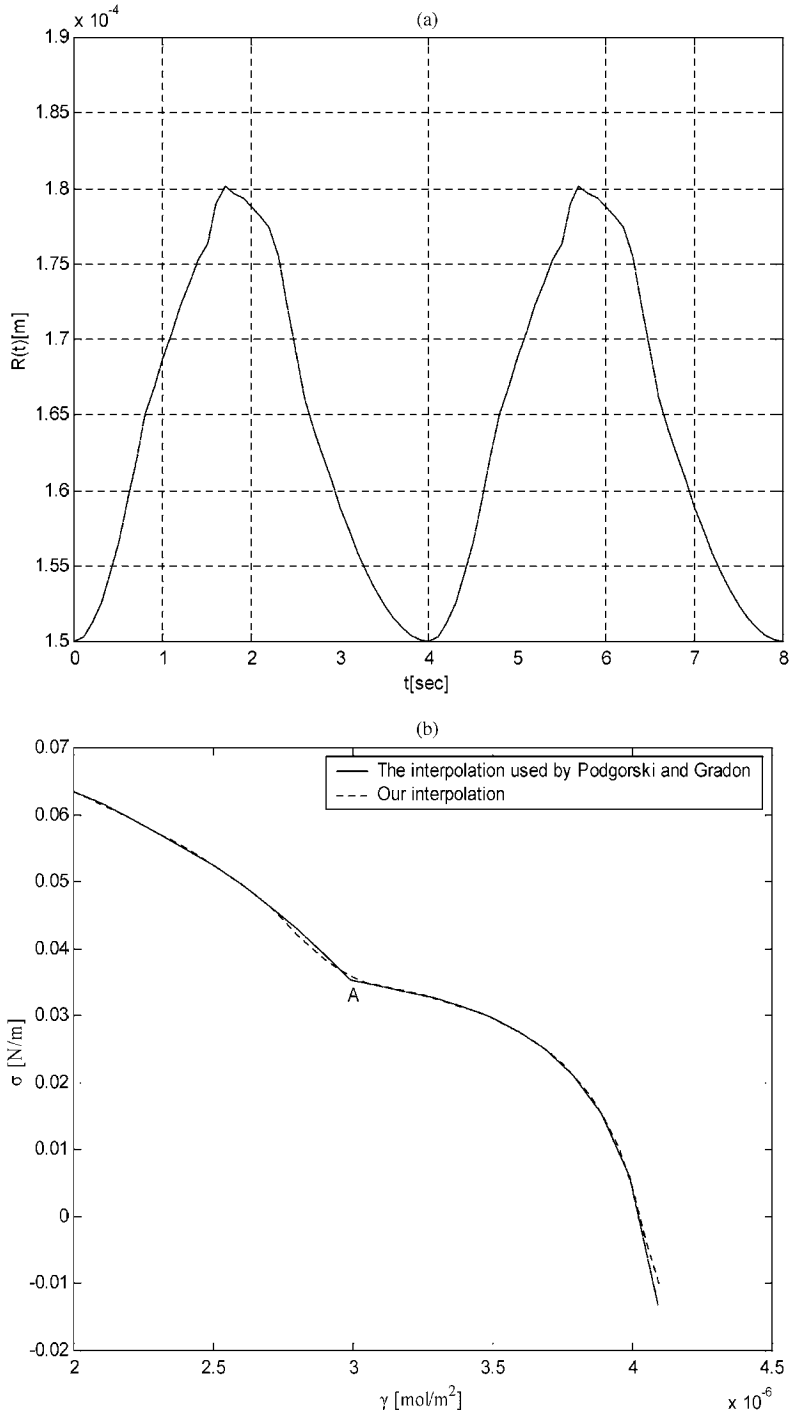

FIG. 2. (a) *Alveolar radius dependency upon time during breathing as suggested in* [22]. *The breathing cycle is* 4 *sec.* (b) *Surface tension dependency upon concentration of the DPPC surfactant. Illustrated are the Podgorski and Gradon* [22] *correlation and the cubic spline interpolation we used in our analysis. Notice that the latter possesses a continuous derivative also at point* A.

amplitude.

Hawgood [15] provided experimental data pertaining to the total amount of surfactant cleared from the rim during a breathing cycle. However, there is practically no data on how the production rate $F(t)$ varies with time and location. With no such prior knowledge, we believe that a leading order approximation can be obtained if we assume that $F(t)$ is expanded in a time Fourier series with period T and consider only the first two leading terms with $F_b(t) \equiv 1$ and $F_{ec}(t) = \sin(\frac{2\pi t}{T})$. This is equivalent to assuming that surfactants are uniformly produced at the alveolus wall and that the rate of excess surfactants leaving the rim is fixed and scales with $\overline{g} = \overline{m}\lambda_b/T$.

According to [15], the amount of surfactant secretion per hour is about 10–40% of the total amount of the surfactant present at the alveolus. If we pick $T = 4$ sec, the amount of surfactant produced per breathing cycle is about $1.1 \cdot 10^{-4}\overline{m}$ to $4.4 \cdot 10^{-4}\overline{m}$. Hawgood [15] also reported that 1–10% of the secreted amount is cleared from the alveolus. Thus, the range of λ_b is $1 \cdot 10^{-6}$–$4 \cdot 10^{-5}$, and that of λ_{ec} is $9 \cdot 10^{-5}$–$3.9 \cdot 10^{-4}$. Henceforth, we set $\lambda_b = 1 \cdot 10^{-5}$ and $\lambda_{ec} = 1.9 \cdot 10^{-4}$ as appropriate scaling values.

The surfactant surface concentration γ scales with $\overline{\gamma} = \overline{m}/2\pi(\overline{R} - \overline{h})^2 d$, where $d = 1 + \cos(\theta_b)$ and thus $\overline{g} = 2\pi\overline{R}^2 d\lambda_b\overline{\gamma}/T$. The velocity of the lining fluid and the diffusion at the interface layer govern the surfactant flux through the rim. Thus, the amount of surfactant leaving the alveolus per unit time is $g = 2\pi(R-h)\sin(\theta_b)(\gamma u_\theta - D\frac{\partial}{\partial\theta}\gamma)_{r=R-h,\theta=\theta_b}$, where $D = 10^{-10}\mathrm{m}^2/\mathrm{sec}$ is the surfactant surface diffusion coefficient (provided in [22]) and u_θ is the tangential surface velocity. Hence, the surface velocity scales with $\overline{u}_\theta = \lambda_b\frac{\overline{R}}{T} \approx 10^{-9}$ m/sec since the flux due to diffusion is of a lesser effect.

Table 1 furnishes a summary of all the additional physical parameters that are employed in the analysis with mean numerical values taken from [10], [15], and [22].

3. Flow equations, boundary conditions, dimensionless parameters and controlling variables. The differential equations that govern the flow of the lining fluid layer are the following:

(a) The continuity equation for an incompressible fluid,

$$\nabla \cdot \mathbf{u} = 0. \tag{1}$$

(b) The quasi-steady linear momentum equation (neglecting body forces and the disjoint pressure),

$$\mu\nabla^2\mathbf{u} = \nabla p. \tag{2}$$

Here, the local acceleration and convection terms have been neglected since the Reynolds numbers, $R_{eT} = \overline{h}^2/Tv = 5 \times 10^{-10}$, $R_{e\theta} = \overline{u}_\theta\overline{h}/v = 4 \times 10^{-11}$, and $R_{er} = |(\overline{u}_r - \dot{\overline{R}})\overline{h}/v| = 10^{-6}$, are much smaller than unity. The disjoint pressure effect may be neglected since the time scale of an instability (Oron, Davis, and Bankoff [18]) that may cause rupture of the thin lining layer is of the order $96\pi^3\overline{h}^5\rho v\overline{\sigma}/A^2 = 100$ sec (for a Hamaker constant A of the order of 10^{-20} J and surface tension as low as $\overline{\sigma} = 1$ dyne/cm), a much slower process than the breathing cycle of 4 seconds. In addition, Wit, Gallez, and Christov [28] concluded that the cutoff wave number is independent of the Marangoni effect.

(c) The mass conservation equation for the surfactant layer is (see Aris [3, p. 86] for the Reynolds transport theorem in a two-dimensional curved space)

TABLE 1
Geometrical and phenomenological properties.

Description	**Typical Value [units]**
Lining fluid thickness	$\overline{h} = 5 \cdot 10^{-8}$ [m]
Alveolar radius	$\overline{R} = 1.6 \cdot 10^{-4}$ [m]
Breathing period	$\overline{t} = 4$ [sec]
Lining fluid outflow velocity	$\overline{u}_\theta = \dfrac{\lambda_b \overline{R}}{\overline{t}} \approx 10^{-9}$ [m/sec]
Surface tension	$\overline{\sigma} = 2.5 \cdot 10^{-2}$ [N/m]
Surfactant concentration at the fluid-air-interface	$\overline{\gamma} = 3.3 \cdot 10^{-6}$ [mol/m^2]
Capillary pressure	$\overline{P} = \dfrac{\overline{\sigma}}{\overline{R}} \approx 156$ [N/m^2]
Amount of surfactants in the lining fluid interface	$\overline{m} = 2\pi \overline{R}^2 d\overline{\gamma} \approx 5 \cdot 10^{-13} d$ [mol]
Ratio of lining fluid thickness to alveolar radius	$\varepsilon = \dfrac{\overline{h}}{\overline{R}} \approx 3 \cdot 10^{-4}$
Ratio of amount of surfactant leaving the alveolus during a breathing period to $\overline{m}$	$\lambda_b = 10^{-5}$
Ratio of amount of surfactant staying in the lining fluid to $\overline{m}$	$\lambda_{ec} = 1.9 \cdot 10^{-4}$
Diffusion coefficient of the surfactants at the fluid interface	$D = 10^{-10}$ [m^2/sec]
Modified capillary number	$\overline{C}_a = \dfrac{\mu \overline{R}^2}{\overline{h}\overline{\sigma} T} = 0.0614$
Alveolus fluid viscosity	$\mu = 12 \cdot 10^{-3}$ [Pa $\cdot$ sec]

$$\mathbf{n} \cdot \frac{\partial(\gamma \mathbf{n})}{\partial t} + \mathbf{u}_s \cdot \nabla_s(\gamma \mathbf{n}) \cdot \mathbf{n} - \gamma \mathbf{n} \cdot (\nabla \mathbf{u}) \cdot \mathbf{n} = D \nabla_s^2 \gamma + \frac{F(t)}{2\pi (R-h)^2 d}, \tag{3}$$

where $\mathbf{n}$ is a unit vector perpendicular to the interface, $\nabla_s = (\mathbf{I} - \mathbf{nn}) \cdot \nabla$ is the surface gradient, $\mathbf{u}_s = (\mathbf{I} - \mathbf{nn}) \cdot \mathbf{u}$ is the surface velocity, and $\mathbf{I}$ is the idem dyadic. The second term on the right-hand side of (3) is a source term that accounts for the amount of surfactant entering the interface from the fluid bulk.

(d) The equation that governs the fluid layer interface location $h(\theta, t)$ is

$$\frac{\partial E}{\partial t} + \mathbf{u} \cdot \nabla E = 0, \tag{4}$$

where $E = r - R(t) + h(\theta, t) = 0$, $\mathbf{n} = \nabla E / |\nabla E|$, and the time derivative is taken for r and θ held fixed.

Assuming that the problem is axisymmetric, (1)–(4) constitute an appropriate set of equations for the five unknown fields p, γ and h, u_r, and u_θ. The latter fields are subject to the following boundary conditions:

$$u_r = \dot{R} - \frac{\lambda_b \overline{R} \hat{U}(t)}{T}, \quad u_\theta = 0, \qquad r = R(t), \tag{5a,b}$$

$$\text{(6a,b)} \qquad \frac{\partial u_r}{\partial \theta} = 0, \quad u_\theta = 0, \qquad \theta = \pi,$$

$$\text{(7)} \qquad \mathbf{n} \cdot \boldsymbol{\tau} \cdot \mathbf{t} = \mathbf{t} \cdot \nabla \sigma, \qquad r = R - h,$$

$$\text{(8)} \qquad p - p_a - \mathbf{n} \cdot \boldsymbol{\tau} \cdot \mathbf{n} - \sigma \nabla \cdot \mathbf{n} = 0, \qquad r = R - h,$$

$$\text{(9)} \qquad \frac{\partial \gamma}{\partial \theta} = 0, \qquad \theta = \pi, \quad r = R - h,$$

$$\text{(10)} \qquad 2\pi r \sin(\theta_b) \left[\gamma u_\theta - \left(\frac{D}{r} \right) \frac{\partial \gamma}{\partial \theta} \right] = -\frac{\overline{m} \lambda_b}{T}, \qquad \theta = \theta_b, \quad r = R - h,$$

where σ stands for the surface tension at the surfactant layer, $\boldsymbol{\tau} = \mu[\nabla \mathbf{u} + (\nabla \mathbf{u})^T]$ is the viscous part of the stress tensor, and $\mathbf{t}$ stands for a unit vector tangential to the interface.

Equation (5a) accounts for the unknown velocity of lining fluid $U = \lambda_b \overline{R} \hat{U}(t)/T$ that is generated at the alveolus boundary and compensates for fluid leaving the alveolus every period. We made here the reasonable assumptions that the production rate scales with the amount of surfactants leaving the alveolus and that the fluid is generated uniformly at the alveolus wall. Equation (5b) is a manifestation of the no-slip condition imposed on the flow, (6a,b) and (9) result from the geometrical symmetry of the alveolus, and (7) represents the jump condition in the tangential component of the stress tensor due to surface tension gradients. Equation (8) considers the jump condition in the normal component of the stress tensor stemming from interface curvature, and (10) demonstrates that a given amount of surfactant leaves the alveolus during every breathing period. (That excess amount is produced at the alveolus wall and diffuses through the lining fluid toward the interface.)

To achieve closure of the problem, it seems that we need an additional boundary condition at $\theta = \theta_b$. However, for very thin fluid layers, lubrication theory applies, and such a condition is redundant. The initial conditions are

$$\text{(11)} \qquad h = \overline{h}, \qquad \gamma = \overline{\gamma},$$

where $\overline{h}$ and $\overline{\gamma}$ are constants and stand for the respective fluid layer thickness and surfactant concentration evaluated at time $t = \overline{t}$ at which the alveolar radius R assumes the value $\overline{R}$.

It shall be demonstrated that a periodic solution is readily obtained for any physical values of $\overline{h}$ and $\overline{\gamma}$. A specific set of initial conditions is required to initiate the numerical scheme but is of no consequence in the final periodic solution. For the sake of convenience, we shall assume that $\overline{t} = 0$.

Based upon experimental observations (Philips and Chapman [21]), a constitutive equation $\sigma = \sigma(\gamma)$ was suggested by Gradon and Podgorski [11], which correlates surface tension to the concentration of DPPC (diacylphosphatidylcholine). The correlation function (Figure 2(b)) includes two smooth regions and a dividing point (A) at which the function is not differentiable. The latter fact results in an aphysical, discontinuous velocity solution near the dividing point. To circumvent this difficulty, we employ a smooth, natural, cubic spline interpolation function that matches well with the Podgorski and Gradon [22] data outside A, predicts a slightly higher value near A, and is differentiable everywhere (see Figure 2(b)).

To render the differential equations and boundary conditions dimensionless, we define the following dimensionless variables (denoted henceforth with a caret symbol):

$$\hat{y} = \frac{(R-r)}{\overline{h}}, \qquad \hat{t} = \frac{t}{T}, \qquad \hat{\nabla}_s = \overline{R}\nabla_s, \qquad \hat{R} = \frac{R(\hat{t})}{\overline{R}},$$

$$\hat{u}_y = \frac{(\dot{R}-u_r)T}{\overline{h}}, \qquad \hat{\sigma} = \frac{\sigma}{\overline{\sigma}}, \qquad \hat{u}_\theta = \frac{u_\theta T}{\overline{R}}, \tag{12}$$

$$\hat{p} = \frac{(p_a - p)\overline{R}}{\overline{\sigma}}, \qquad \hat{\gamma} = \frac{\gamma}{\overline{\gamma}}, \qquad \hat{h} = \frac{h}{\overline{h}}.$$

Substituting (12) into (1)–(11) yields an equivalent set of dimensionless equations and boundary conditions, where the dimensionless unknowns depend on the independent variables $\hat{y}$, θ, $\hat{t}$ and parameters λ_b, λ_{ec}, ε, P_e, C_a, θ_b. Here $\varepsilon = \overline{h}/\overline{R} = 3 \times 10^{-4}$ is the lining fluid depth ratio, $P_e = \overline{R}^2/DT = 64$ stands for the Peclet number, and $C_a = \mu\overline{u}_\theta/\overline{\sigma} = 4.8 \times 10^{-11}$ is the capillary number. Equations (1)–(4) are highly nonlinear and couple the velocity field with surfactant concentration and the location of the interface. In the next chapter, we employ an asymptotic expansion in the two smallness parameters λ_b, ε, which makes it possible to solve the problem semianalytically.

4. The asymptotic formulation. A possible clue for a coherent asymptotic representation of the unknown functions is that the cleansing mechanism results from the generation of an excess amount of surfactant determined by λ_b, a parameter that plays a paramount role in the solution. The value of λ_b is of the order of 10^{-5}; thus gradients in surface tension driving the flow are expected to be very small, albeit not zero, resulting in a nonzero small tangential velocity. Had λ_b vanished, the lining fluid would have remained inside the alveolus at all times, covered the alveolus wall uniformly, and grown thicker during exhalation and thinner during inhalation to conserve mass. In this case, the unknown functions h, γ, σ, p, and $\mathbf{u}$ would have been radially symmetric, i.e., depended upon t but not upon θ. Consequently, the following regular asymptotic expansions in λ_b and ε are suggested:

$$\hat{u}_y = \overset{0}{u}_y\,(\hat{y},\hat{t};\varepsilon) + \lambda_b[\hat{U}_y(\hat{y},\theta,\hat{t}) + \varepsilon\hat{U}_y^{(1)}(\hat{y},\theta,\hat{t}) + \cdots] + O(\lambda_b^2), \tag{13a}$$

$$\hat{u}_\theta = \lambda_b[\hat{U}_\theta(\hat{y},\theta,\hat{t}) + \varepsilon\hat{U}_\theta^{(1)}(\hat{y},\theta,\hat{t}) + \cdots] + O(\lambda_b^2), \tag{13b}$$

$$\hat{h} = \overset{0}{h}\,(\hat{t};\varepsilon) + \lambda_b[\hat{H}(\theta,\hat{t}) + \varepsilon\hat{H}^{(1)}(\theta,\hat{t}) + \cdots] + O(\lambda_b^2), \tag{13c}$$

$$\hat{\gamma} = \overset{0}{\gamma}\,(\hat{t};\varepsilon) + \lambda_b[\hat{\Gamma}(\theta,\hat{t}) + \varepsilon\hat{\Gamma}^{(1)}(\theta,\hat{t}) + \cdots] + O(\lambda_b^2), \tag{13d}$$

$$\hat{\sigma} = \overset{0}{\sigma}\,(\hat{t};\varepsilon) + \lambda_b[\hat{\Sigma}(\theta,\hat{t}) + \varepsilon\hat{\Sigma}^{(1)}(\theta,\hat{t}) + \cdots] + O(\lambda_b^2), \tag{13e}$$

$$\hat{p} = \overset{0}{p}\,(\hat{t};\varepsilon) + \lambda_b[\hat{P}(\theta,\hat{t}) + \varepsilon\hat{P}^{(1)}(\theta,\hat{t}) + \cdots] + O(\lambda_b^2). \tag{13f}$$

Here, the naught symbol denotes the radially symmetric solution, and uppercase symbols are used to denote asymptotic, first order fields in λ_b. Notice that the leading term $\overset{0}{u}_\theta$ vanishes identically in expansion (13b); i.e., a tangential velocity component stems solely from excess production of surfactant (see also section 3).

Henceforth, we shall focus our attention on the first two terms in the foregoing expansions and neglect the contribution of the third, order $O(\lambda_b\varepsilon)$, much smaller term. Substituting (13) into the dimensionless form of (1)–(11) and collecting the zero and first order terms in λ_b results in two respective sets of dimensionless differential equations and boundary conditions.

4.1. The zero order approximation. For the zero order, radially symmetric fields, the equations are as follows:
the continuity equation,

$$\frac{\partial}{\partial\hat{y}}\left[(\hat{R}-\varepsilon\hat{y})^2\left(\frac{d\hat{R}}{d\hat{t}}-\varepsilon\overset{0}{u}_y\right)\right]=0, \tag{14a}$$

the radial momentum equation,

$$\frac{1}{(\hat{R}-\varepsilon\hat{y})^2}\left\{\frac{\partial}{\partial\hat{y}}\left[(\hat{R}-\varepsilon\hat{y})^2\frac{\partial\overset{0}{u}_y}{\partial\hat{y}}\right]+2\varepsilon\left(\frac{d\hat{R}}{d\hat{t}}-\varepsilon\overset{0}{u}_y\right)\right\}=-\left(\frac{\overline{T}\overline{\sigma}}{\mu\overline{R}}\right)\frac{\partial\overset{0}{p}}{\partial\hat{y}}, \tag{14b}$$

the mass conservation equation of surfactants,

$$\frac{\partial\overset{0}{\gamma}}{\partial\hat{t}}-\overset{0}{\gamma}\left.\frac{\partial\overset{0}{u}_y}{\partial\hat{y}}\right|_{\hat{y}=\overset{0}{h}}=\frac{1}{(\hat{R}-\varepsilon\overset{0}{h})^2}\lambda_{ec}\sin(2\pi\hat{t}), \tag{14c}$$

and the kinematic condition for interface location,

$$\frac{\partial\overset{0}{h}}{\partial\hat{t}}=\left.\overset{0}{u}_y\right|_{\hat{y}=\overset{0}{h}}. \tag{14d}$$

The appropriate boundary conditions are

$$\overset{0}{u}_y=0,\qquad \hat{y}=0, \tag{15a}$$

$$\overset{0}{p}=\frac{2\overset{0}{\sigma}}{(\hat{R}-\varepsilon\overset{0}{h})},\qquad \hat{y}=\overset{0}{h}. \tag{15b}$$

The initial conditions are replaced by the requirement that the solution be periodic.

Notice that the foregoing equations are not expanded with respect to ε, since, as shall be demonstrated in the next section, an exact solution of (14) is feasible for any value of ε.

4.2. The first order approximation. Substituting (13) into (1)–(10) and collecting first order terms in λ_b yields the following set of equations and boundary conditions:
the continuity equation,

$$\hat{R}\frac{\partial}{\partial\hat{y}}\hat{U}_y+\frac{\partial}{\partial\theta}\hat{U}_\theta+\cot(\theta)\hat{U}_\theta=0, \tag{16a}$$

the momentum equation in the radial direction,

$$\frac{\partial \hat{P}}{\partial \hat{y}} = 0, \tag{16b}$$

the momentum equation in the tangential direction,

$$\frac{\partial^2 \hat{U}_\theta}{\partial \hat{y}^2} = 0, \tag{16c}$$

the mass conservation equation of surfactants,

$$\hat{R}^2 \frac{\partial \hat{\Gamma}}{\partial \hat{t}} + 2\hat{R}\hat{\Gamma}\frac{d\hat{R}}{d\hat{t}} - \frac{\partial \hat{U}_y}{\partial \hat{y}} - \frac{1}{P_e}\left[\frac{\partial^2 \hat{\Gamma}}{\partial \theta^2} + \cot(\theta)\frac{\partial \hat{\Gamma}}{\partial \theta}\right] = 1, \tag{16d}$$

and the kinematic condition for interface location,

$$\frac{\partial \hat{H}}{\partial \hat{t}} = [\hat{U}_y]_{\hat{y}=\overset{0}{h}}. \tag{16e}$$

Notice that time derivatives in (16d,e) are carried out for y and θ held fixed. The appropriate boundary conditions are

$$\hat{U}_y = \hat{U}, \qquad \hat{y} = 0, \tag{17a}$$

$$\hat{U}_\theta = 0, \qquad \hat{y} = 0, \tag{17b}$$

$$\frac{\partial \hat{\Gamma}}{\partial \theta} = 0, \qquad \theta = \pi, \tag{17c}$$

$$\frac{\partial \hat{U}_y}{\partial \theta} = 0, \qquad \theta = \pi, \tag{17d}$$

$$\hat{U}_\theta = 0, \qquad \theta = \pi, \tag{17e}$$

$$\overline{C}_a^{-1}\frac{\partial \hat{\Sigma}}{\partial \theta} - \hat{R}\frac{\partial \hat{U}_\theta}{\partial \hat{y}} = 0, \qquad \hat{y} = \frac{1}{\hat{R}^2}, \tag{17f}$$

$$\hat{P} = 0, \qquad \hat{y} = \frac{1}{\hat{R}^2}, \tag{17g}$$

$$\hat{R}\left[\overset{0}{\gamma}\hat{U}_\theta - \frac{1}{P_e\hat{R}}\frac{\partial \hat{\Gamma}}{\partial \theta}\right] = -\cot\left(\frac{\theta_b}{2}\right), \qquad \theta = \theta_b,\ r = R - h, \tag{17h}$$

where $\overline{C}_a = \frac{\mu \overline{R}/T}{\overline{\sigma}}\frac{\overline{R}}{\overline{h}} = 0.0614$ is the modified capillary number whose inverse scales the Marangoni effect. Notice that $\overline{C}_a$ is the governing capillary number that results from the balance between the shear forces and the surface tension gradients at the interface (17f). A velocity scale defined by $\overline{R}/T$ would be improper since it governs the zero order radially symmetric fields.

In the next section, solutions for the zero and first order approximation fields are addressed.

5. The solution of the zero and first order perturbations.

5.1. The zero order, radially symmetric solution. The exact solutions for the radially symmetric fields (14a–d) are[1]

$$\overset{0}{u}_y = \frac{1}{\varepsilon}\frac{d\hat{R}}{d\hat{t}}\left(1 - \frac{\hat{R}^2}{(\hat{R}-\varepsilon\hat{y})^2}\right) = -2\frac{\hat{y}}{\hat{R}}\frac{d\hat{R}}{d\hat{t}} + O(\varepsilon), \tag{18a}$$

$$\overset{0}{p} = \frac{2\hat{\sigma}(\overset{0}{\gamma})}{(\hat{R}-\varepsilon\overset{0}{h})}, \tag{18b}$$

$$\overset{0}{h} = \frac{1}{\varepsilon}[\hat{R} - (\hat{R}^3 - 1 + (1-\varepsilon)^3)^{1/3}] = \frac{1}{\hat{R}^2} + O(\varepsilon), \tag{18c}$$

$$\overset{0}{\gamma} = \frac{(1-\varepsilon)^2}{(\hat{R}-\varepsilon\overset{0}{h})^2}\left(1 - \frac{\lambda_{ec}}{2\pi}\cos\left[2\pi\left(\hat{t} - \frac{\bar{t}}{T}\right)\right]\right) = \frac{1}{\hat{R}^2} + O(\lambda_{ec}) + O(\varepsilon). \tag{18d}$$

Notice that the radially symmetric pressure is uniform across the lining layer and that for small values of ε the leading terms of the radially symmetric solutions are of order unity.

5.2. The first order perturbation in $\boldsymbol{\lambda_b}$. The solution of (16a–e)–(17a–h) is divided into two consecutive steps. First, an analytic expression is obtained for the velocity $\hat{U}_\theta$, which is substituted into (16d). A numerical scheme is then employed, in which a finite-element method is utilized along θ and a finite difference predictor-corrector method is employed along t to solve the transformed equation (16d).

Integrating (17f) and (16c) and employing boundary condition (17b) yields

$$\hat{U}_\theta = \hat{W}(\theta,\hat{t})\hat{y}. \tag{19a}$$

From (16d), the unknown function $\hat{W}(\theta,\hat{t})$ can easily be determined in terms of $\hat{\Sigma}$ or $\hat{\Gamma}$:

$$\hat{W}(\theta,t) = \frac{\overline{C}_a^{-1}}{\hat{R}}\frac{\partial\hat{\Sigma}}{\partial\theta} = \frac{\overline{C}_a^{-1}}{\hat{R}}\frac{\partial\hat{\sigma}}{\partial\hat{\gamma}}\bigg|_{\hat{\gamma}=1/\hat{R}^2}\frac{\partial\hat{\Gamma}}{\partial\theta}. \tag{19b}$$

The latter equality stems from the known constitutive relation between surface tension and surfactant concentration.

Introducing (16a) into (16d) and employing (19a) and (19b) yields the second order partial differential equation in $\hat{\Gamma}$,

$$\frac{\partial(\hat{R}^2\hat{\Gamma})}{\partial\hat{t}} + \left[\frac{\overline{C}_a^{-1}}{\hat{R}^4}\frac{\partial\hat{\sigma}}{\partial\hat{\gamma}}\bigg|_{\hat{\gamma}=1/\hat{R}^2} - \frac{1}{P_e}\right]\left[\frac{\partial^2\hat{\Gamma}}{\partial\theta^2} + \cot(\theta)\frac{\partial\hat{\Gamma}}{\partial\theta}\right] = 1, \tag{20a}$$

subject to the boundary conditions

$$\frac{\partial\hat{\Gamma}}{\partial\theta} = 0, \qquad \theta = \pi, \tag{20b}$$

[1] An easy route to obtaining the exact solutions is to consider the problem from a global point of view in which the total fluid and surfactant mass during breathing is conserved.

$$\left(\frac{\overline{C}_a^{-1}}{\hat{R}^4}\frac{\partial\hat{\sigma}}{\partial\hat{\gamma}}\bigg|_{\hat{\gamma}=1/\hat{R}^2} - \frac{1}{P_e}\right)\frac{\partial\hat{\Gamma}}{\partial\theta} = -\cot\left(\frac{\theta_b}{2}\right), \qquad \theta=\theta_b, \tag{20c}$$

and the initial condition

$$\hat{\Gamma} = 0. \tag{20d}$$

Notice that since $\partial\hat{\sigma}/\partial\hat{\gamma}$ is invariably negative, (20a) possesses the form of a diffusion equation with an effective time dependent diffusion coefficient that is always positive.

To simplify the finite-element formulation of the problem, we rewrite (20a) and (20c):

$$A(\hat{t})\frac{\partial\hat{\Gamma}}{\partial\hat{t}} + B(\hat{t})\hat{\Gamma} + C(\hat{t})\left(\frac{\partial^2}{\partial\theta^2}\hat{\Gamma} + \cot(\theta)\frac{\partial\hat{\Gamma}}{\partial\theta}\right) = 1, \qquad \pi<\theta<\theta_b, \tag{21a}$$

$$\frac{\partial\hat{\Gamma}}{\partial\theta} = G(\hat{t}), \qquad \theta=\theta_b, \tag{21b}$$

where

$$\begin{aligned} A(\hat{t}) &= \hat{R}^2, \\ B(\hat{t}) &= 2\hat{R}\frac{d\hat{R}}{d\hat{t}}, \\ C(\hat{t}) &= \frac{\overline{C}_a^{-1}}{\hat{R}^4}\frac{\partial\hat{\sigma}}{\partial\hat{\gamma}}\bigg|_{\hat{\gamma}=1/\hat{R}^2} - \frac{1}{P_e}, \\ G(\hat{t}) &= -\left(\frac{\overline{C}_a^{-1}}{\hat{R}^4}\frac{\partial\hat{\sigma}}{\partial\hat{\gamma}}\bigg|_{\hat{\gamma}=1/\hat{R}^2} - \frac{1}{P_e}\right)^{-1}\cot\left(\frac{\theta_b}{2}\right). \end{aligned} \tag{21c}$$

The equation governing the deviation of the interface from its spherical shape $\hat{H}$ is obtained from (16a,e) and (19a,b),

$$\frac{\partial\hat{H}}{\partial\hat{t}} = \frac{\hat{U}}{\hat{R}} - \frac{\overline{C}_a^{-1}}{2\hat{R}^6}\frac{\partial\hat{\sigma}}{\partial\hat{\gamma}}\bigg|_{\hat{\gamma}=1/\hat{R}^2}\left(\frac{\partial^2\hat{\Gamma}}{\partial\theta^2} + \cot(\theta)\frac{\partial\hat{\Gamma}}{\partial\theta}\right). \tag{22}$$

Little is known about the spatial distribution and the time evolution of $\hat{U}$. A global mass-conservation requires that the amount of fluid generated at the alveolus wall equal the amount exiting the alveolus during a single breathing period. Consequently,

$$\int_0^T\left(2\pi R\sin(\theta_b)\int_0^h u_\theta dy\right)dt = \lambda_b\frac{\overline{R}}{T}\int 2\pi R^2[1+\cos(\theta_b)]\hat{U}dt. \tag{23}$$

Substituting (19a,b) into (23) yields

$$\int_0^1 \hat{R}^2\hat{U}d\hat{t} = \frac{1}{2}\varepsilon\overline{C}_a^{-1}\tan\left(\frac{\theta_b}{2}\right)\int_0^1\frac{1}{\hat{R}^4}\frac{\partial\hat{\sigma}}{\partial\hat{\gamma}}\bigg|_{\hat{\gamma}=1/\hat{R}^2}\left[\frac{\partial\hat{\Gamma}}{\partial\theta}\right]_{\theta=\theta_b}dt. \tag{24}$$

Hence $\hat{U}$ is of order ε, and the second term in (22) determines the time evolution and spatial distribution of $\hat{H}$. Fortunately, the equations for $\hat{\Gamma}$ and $\hat{H}$ are decoupled, and we focus on solving $\hat{\Gamma}$, which makes it possible to predict the tangential velocity.

A weak form of the equation for $\hat{\Gamma}$ is obtained by integrating (21a) over the solution domain

$$\int_{\theta=\theta_b}^{\pi} w\left[A(\hat{t})\frac{\partial\hat{\Gamma}}{\partial\hat{t}}+B(\hat{t})\hat{\Gamma}+C(\hat{t})\left(\frac{\partial^2\hat{\Gamma}}{\partial\theta^2}+\cot(\theta)\frac{\partial\hat{\Gamma}}{\partial\theta}\right)-1\right]d\theta=0, \tag{25}$$

where w is any differentiable weighting function. Integrating (25) by parts and utilizing boundary conditions (20b) and (21b) yields

$$\begin{aligned}&\int_{\theta=\theta_b}^{\pi}\left\{w\left[A(\hat{t})\frac{\partial\hat{\Gamma}}{\partial\hat{t}}+B(\hat{t})\hat{\Gamma}+C(\hat{t})\cot(\theta)\frac{\partial\hat{\Gamma}}{\partial\theta}\right]-C(t)\frac{\partial w}{\partial\theta}\frac{\partial\hat{\Gamma}}{\partial\theta}\right\}d\theta\\&=\int_{\theta=\theta_b}^{\pi}wd\theta+w(\theta_b)C(\hat{t})G(\hat{t}).\end{aligned} \tag{26}$$

An element mesh is formed over the solution domain, and w and $\hat{\Gamma}$ are expanded in the following Galerkin sums (see, for example, [17]) for arbitrary c_A's:

$$\begin{aligned}w&=\sum_{A\in\Omega}c_AN_A(\theta),\\\hat{\Gamma}&=\sum_{B\in\Omega}d_B(\hat{t})N_B(\theta),\end{aligned} \tag{27}$$

where Ω denotes the nodes index group and N_A and N_B are the shape functions, $N_1(\theta)$ being the shape function of an element located at the alveolus opening. The unknown time dependent functions $d_B(\hat{t})$ are to be determined as follows. Substituting (27) into (26) yields

$$\begin{aligned}&\sum_{B\in\Omega}\frac{d}{d\hat{t}}d_B\int_{\theta=\theta_b}^{\pi}N_AA(\hat{t})N_Bd\theta\\&\quad+\sum_{B\in\Omega}d_B\int_{\theta=\theta_b}^{\pi}\left\{\begin{array}{l}N_AB(\hat{t})N_B+N_AC(\hat{t})\cot(\theta)\dfrac{dN_B}{d\theta}\\[2ex]-C(\hat{t})\dfrac{dN_A}{d\theta}\dfrac{dN_B}{d\theta}\end{array}\right\}d\theta\\&\quad=\int_{\theta=\theta_b}^{\pi}N_Ad\theta+N_1(\theta_b)C(\hat{t})G(\hat{t}).\end{aligned} \tag{28}$$

Thus (28) possesses the form

$$M\frac{d}{d\hat{t}}d(\hat{t})+Kd(\hat{t})=V, \tag{29}$$

where d is a vector consisting of the unknown functions $d_A(A\in\Omega)$, M and K are

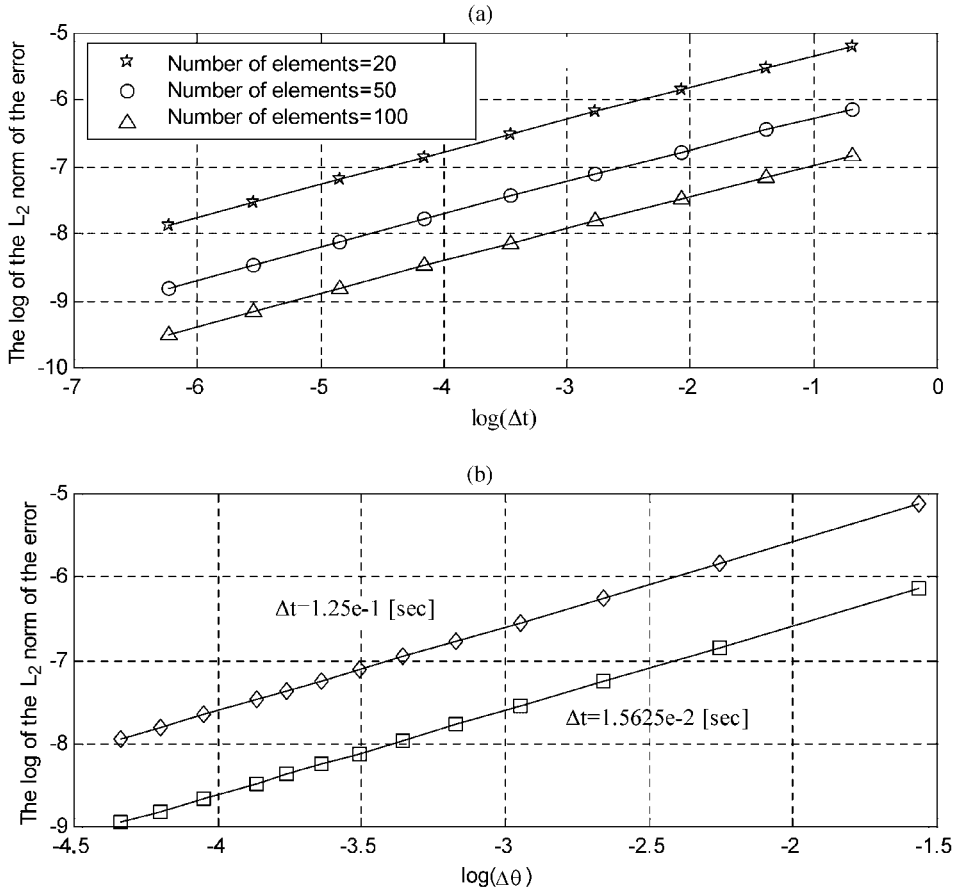

FIG. 3. *Error evaluation for various* (a) *mesh-sizes,* (b) *time-steps. The error is defined by the equation* $L\Gamma_{\text{calculated}} = \text{error}$*, where* L *is the differential operator defined in* (21a).

coefficient matrices, and V is a vector defined as follows:

$$
\begin{aligned}
M_{AB} &= \int_{\theta=\theta_b}^{\pi} N_A A(\hat{t}) N_B d\theta, \\
K_{AB} &= \int_{\theta=\theta_b}^{\pi} \left\{ N_A B(\hat{t}) N_B + N_A C(\hat{t}) \cot(\theta) \frac{dN_B}{d\theta} - C(t) \frac{dN_A}{d\theta} \frac{dN_B}{d\theta} \right\} d\theta, \\
V_A &= \int_{\theta=\theta_b}^{\pi} N_A d\theta + N_1(\theta_b) C(\hat{t}) G(\hat{t}).
\end{aligned} \tag{30}
$$

Choosing linear shape functions N_A, the matrices $M = [M_{AB}]$, $K = [K_{AB}]$ and the vector $V = [V_A]$ can be numerically calculated.

The time evolution equation (29) is numerically solved by a predictor-corrector code. Convergence and error properties of the numerical scheme, the time evolution of the surfactant distribution, the tangential velocities, and the effect of varying the phenomenological parameters are all addressed in the next section.

6. Results. We examined the convergence and accuracy of the numerical scheme; the results are illustrated in Figures 3–5. An L_2 norm was utilized to evaluate errors

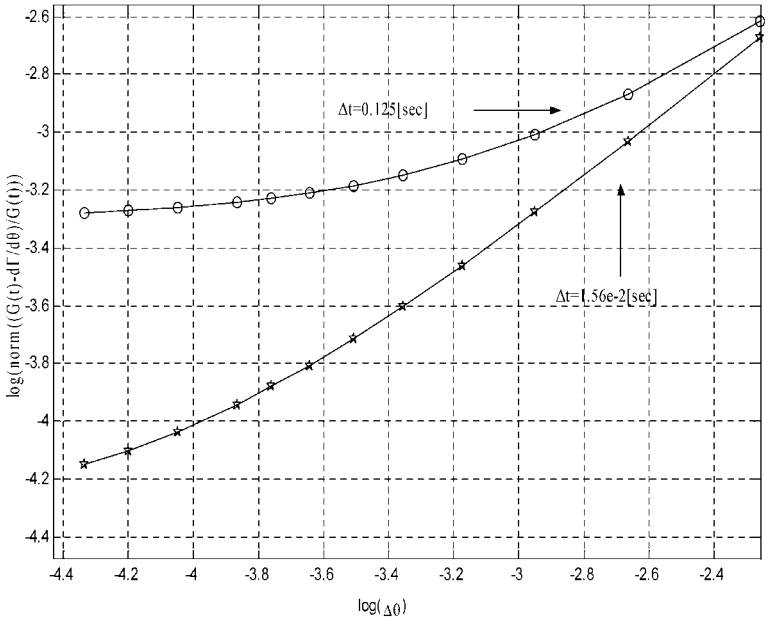

FIG. 4. *The relative error between the calculated derivative* $\partial\Gamma/\partial\theta$ *at* θ_b *and its known exact value from boundary conditions* (21b,c).

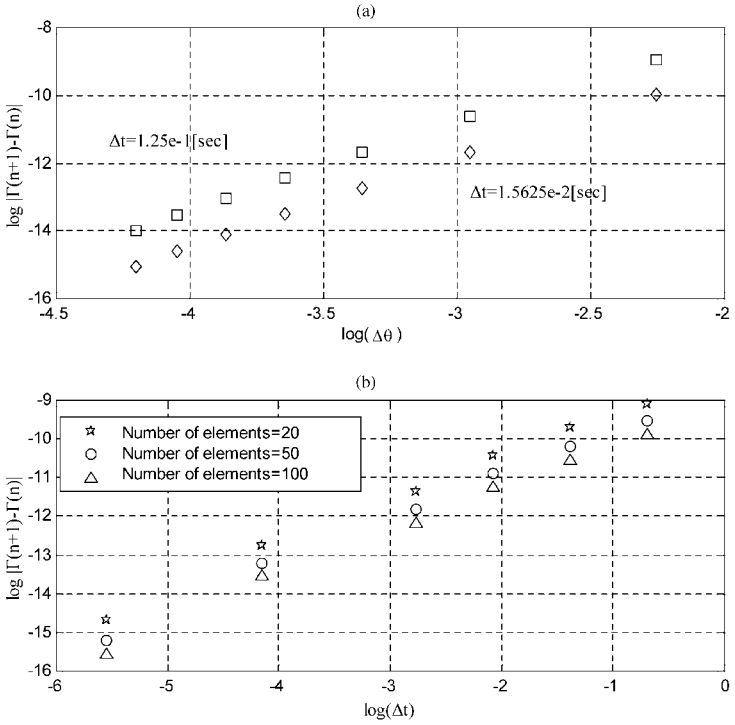

FIG. 5. *Solution convergence for various* (a) *mesh sizes,* (b) *time-steps. Here* $\Gamma(n)$ *is an* L_2 *norm of* Γ *in the solution domain, and* n *defines refinement order.*

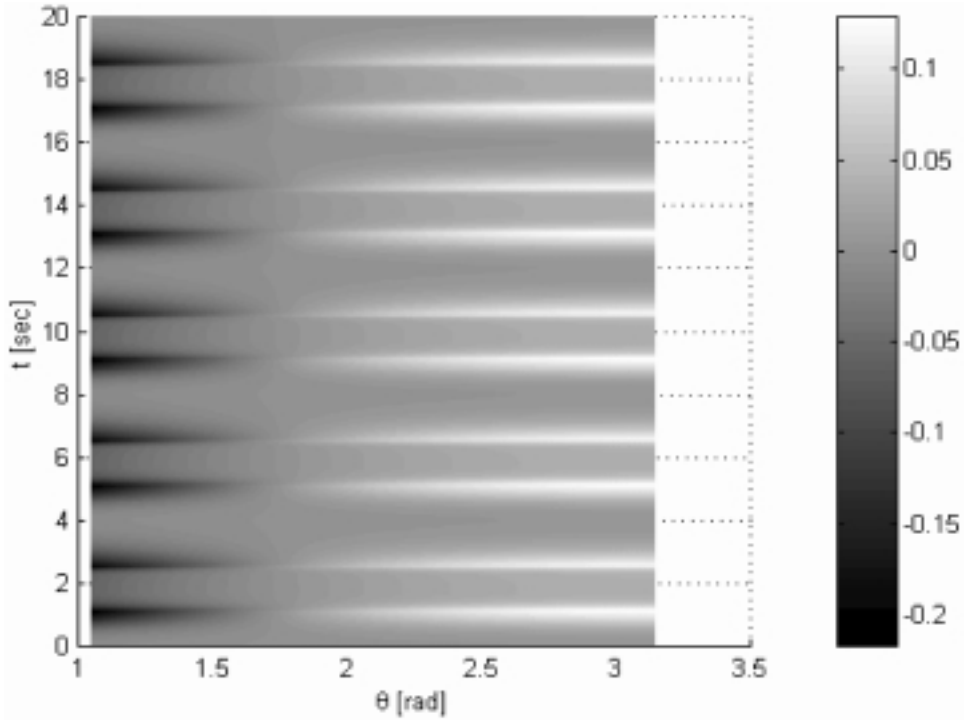

FIG. 6. *Surfactant concentration* Γ *as a function of position and time during five breathing periods.*

in the solution for $\hat{\Gamma}$. To that end, we used the parameter values defined in Table 1; the solution domain was defined by $\pi/3 \leq \theta \leq \pi$; and comparisons were made for the time interval $16 \leq t \leq 20$ sec. The chosen time span, the fifth breathing cycle, was picked to avoid transient effects that may exist at earlier times and are affected by the particular choice of initial conditions. The calculations were repeated for refined time-steps and elements in the θ-direction. We tested grids having 10 to 160 elements in the θ-direction, and time-step sizes ranging between 0.5 sec and $1.95 \cdot 10^{-3}$ sec. The results are summarized in Figure 3, which demonstrates that the estimated error decreases for both time and grid refinements. The best error estimate can be achieved at the boundaries, where a comparison can easily be made between known exact values of the derivatives of $\hat{\Gamma}$ and the respective numerical predictions (see Figure 4). The figure makes clear that the error decreases monotonically with reduced values of time-steps and increased number of elements.

To evaluate the convergence rate of the solution, an L_2 norm was also calculated for the difference between consecutive refined solutions (see Figure 5(a,b)). The figures illustrate vividly that convergence is achieved even for high values of time-steps (of order 0.1) and a small number of elements (of order 20).

Since the solution is approximated up to order ε, no greater precision than 10^{-4} is required. Consequently, from Figures 3–5, a time-step size of 0.015 sec was selected, and the θ-domain was divided into 100 elements, a parameter set that yields a converging solution with an estimated absolute error of order ε or less.

The time evolution of the surfactants and velocity fields is illustrated in Figures 6–10. Since $R(t)$ is a periodic function and, consequently, the time dependent coefficients

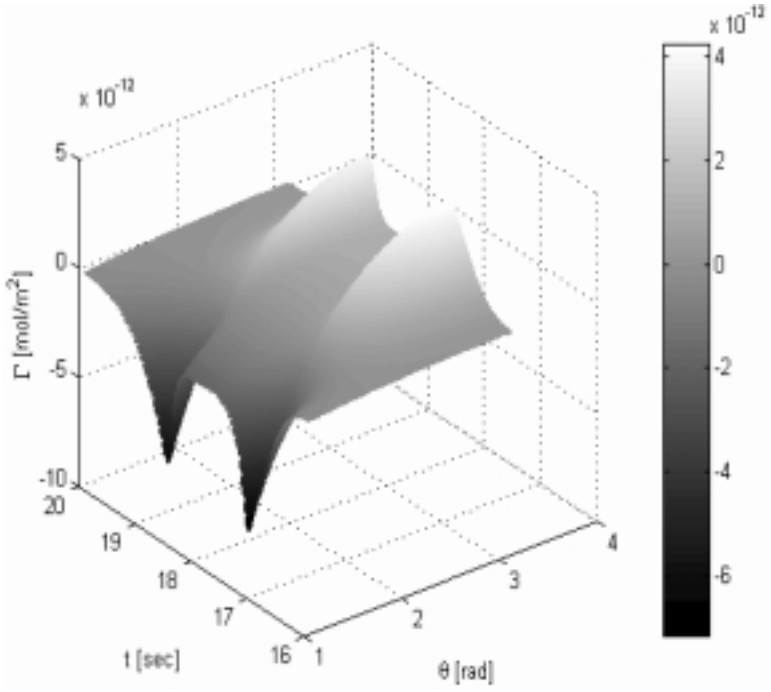

FIG. 7. *Surfactant concentration* Γ *as a function of position and time during the fifth breathing period.*

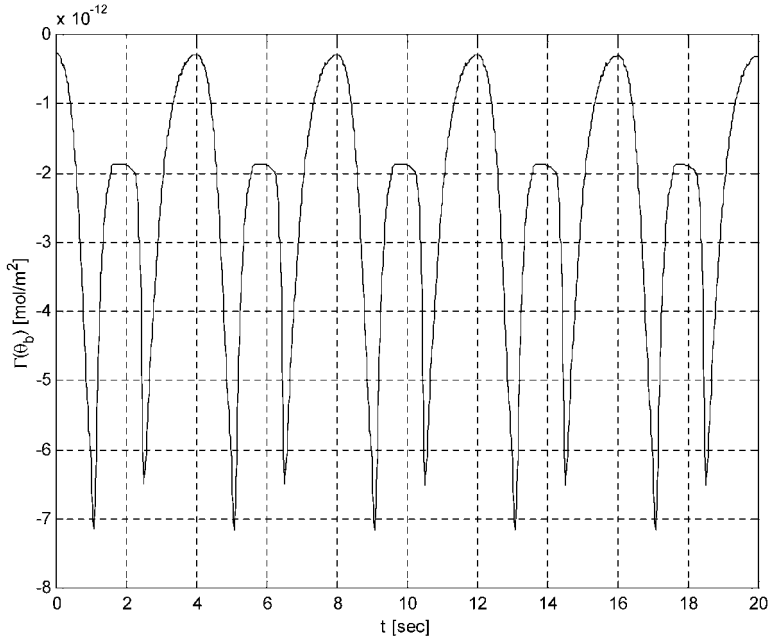

FIG. 8. *The evolution of surfactant concentration* Γ *at* θ_b *during five breathing periods. Notice the two-peak pattern occurring within every breathing period.*

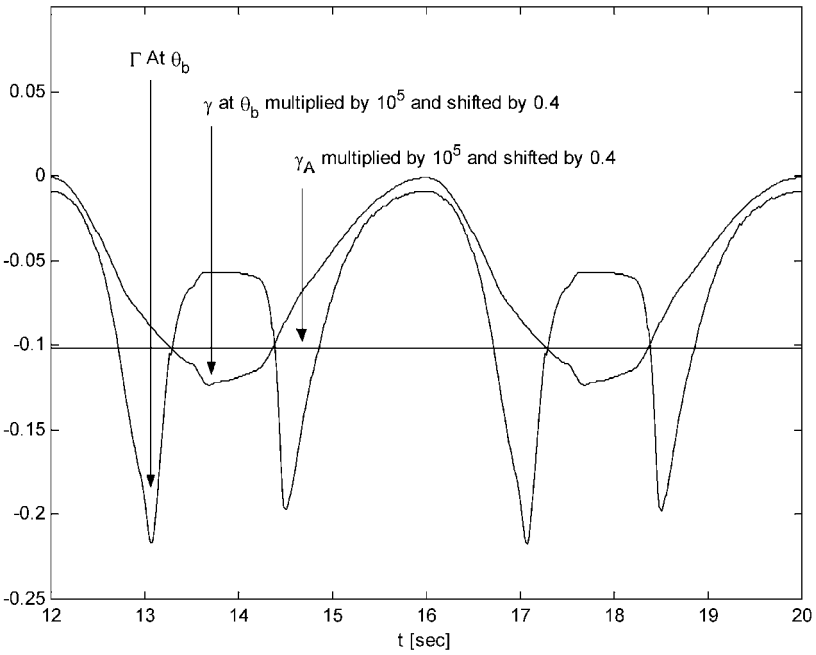

FIG. 9. *The temporal evolution of the radial surfactant concentration* $\overset{0}{\gamma}$ *and* Γ. *Notice that* Γ *reaches a maximum value when* $\gamma = \gamma_A$.

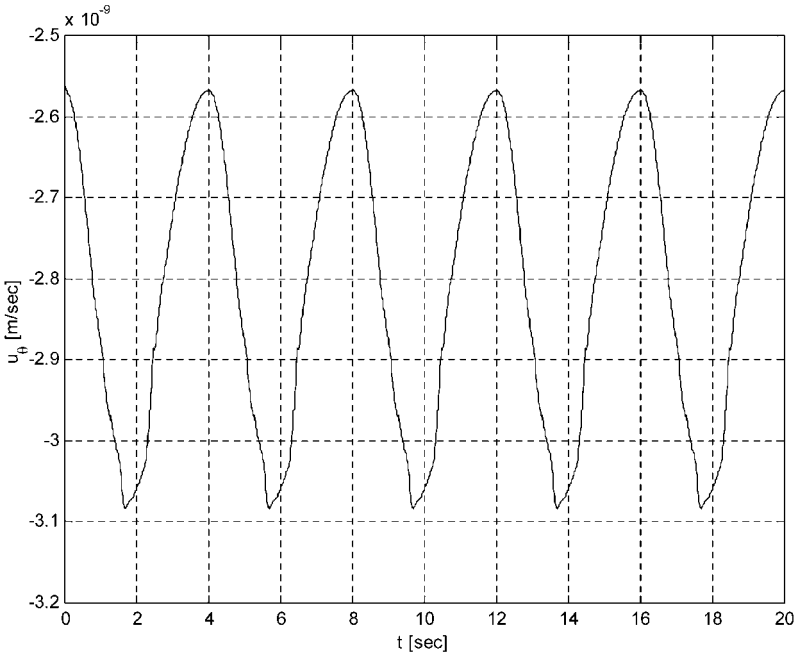

FIG. 10. *The temporal evolution of the tangential velocity* U_θ *at* $\theta_b = \pi/3$.

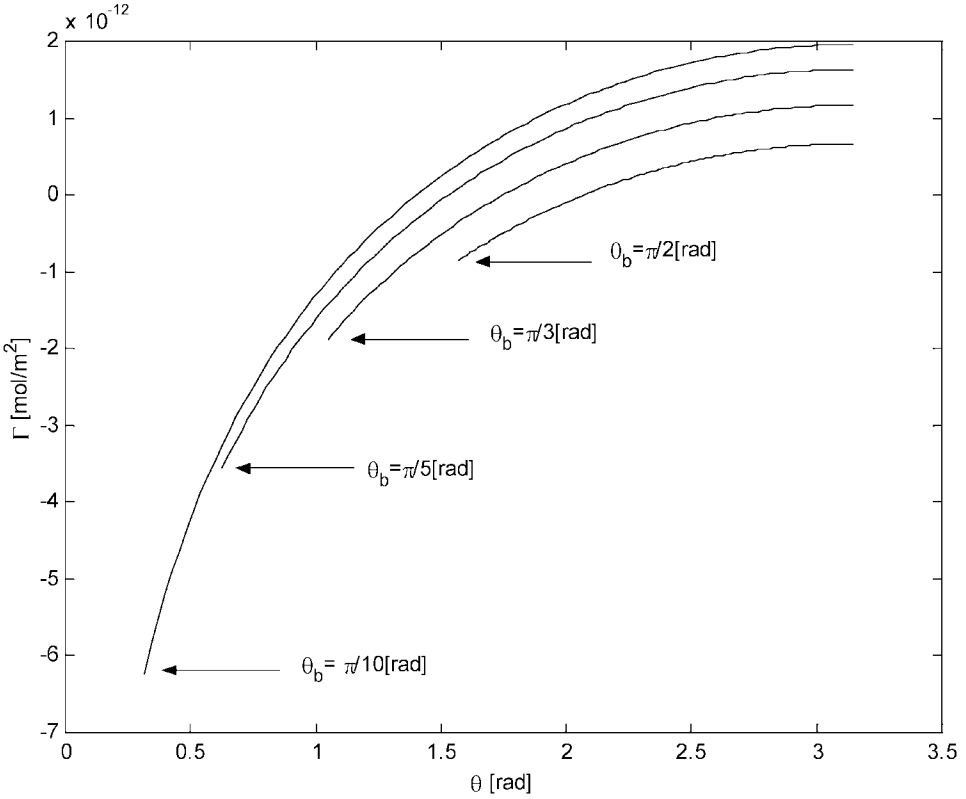

FIG. 11. *The spatial distribution of surfactant concentration* Γ *for various values of* θ_b.

of (20a–d) are periodic, we expect a periodic steady-state solution to the problem. Indeed, Figure 6 demonstrates that $\hat{\Gamma}$ reaches a steady state after a short transient period of less than a single breathing cycle.

During every breathing period, $\hat{\Gamma}$ (at θ_b) possesses a two-peak pattern (see Figures 7 and 8). We use, henceforth, the dimensional form of $\hat{\Gamma}$, namely, $\Gamma = \lambda_b \overline{\gamma} \hat{\Gamma}$, to describe the small perturbation in surfactant concentration. The peaks occur during inhalation and exhalation when the derivative of the surface tension with respect to surfactant concentration varies abruptly as γ crosses point A in Figure 2(b) (see Figure 9). The value of Γ remains negative throughout the breathing process. Thus, the total surfactant concentration $\gamma = \overline{\gamma} \overset{0}{\gamma} + \Gamma$ is lower than its radially symmetric concentration $\overline{\gamma} \overset{0}{\gamma}$. This is reflected in a higher than average surface tension at θ_b and a net fluid motion toward the alveolar edge. The latter conclusion is also illustrated in Figure 10, in which the time dependence of the tangential velocity at the interface is depicted. Notice that a negative value for u_θ means a flow direction toward the alveolar edge (Figure 1). It demonstrates that the velocity is a time-periodic function that possesses a negative mean; namely, there is a net flow exiting the alveolus.

Figures 11 and 12 illustrate a smooth spatial distribution of Γ and u_θ for various values of θ_b. Figure 11 validates the former conclusion that surfactant concentration is lowest (surface tension is highest) at θ_b, namely, fluid is drawn toward the alveolar edge. Figure 12 illustrates that the tangential velocity increases (in absolute value) as

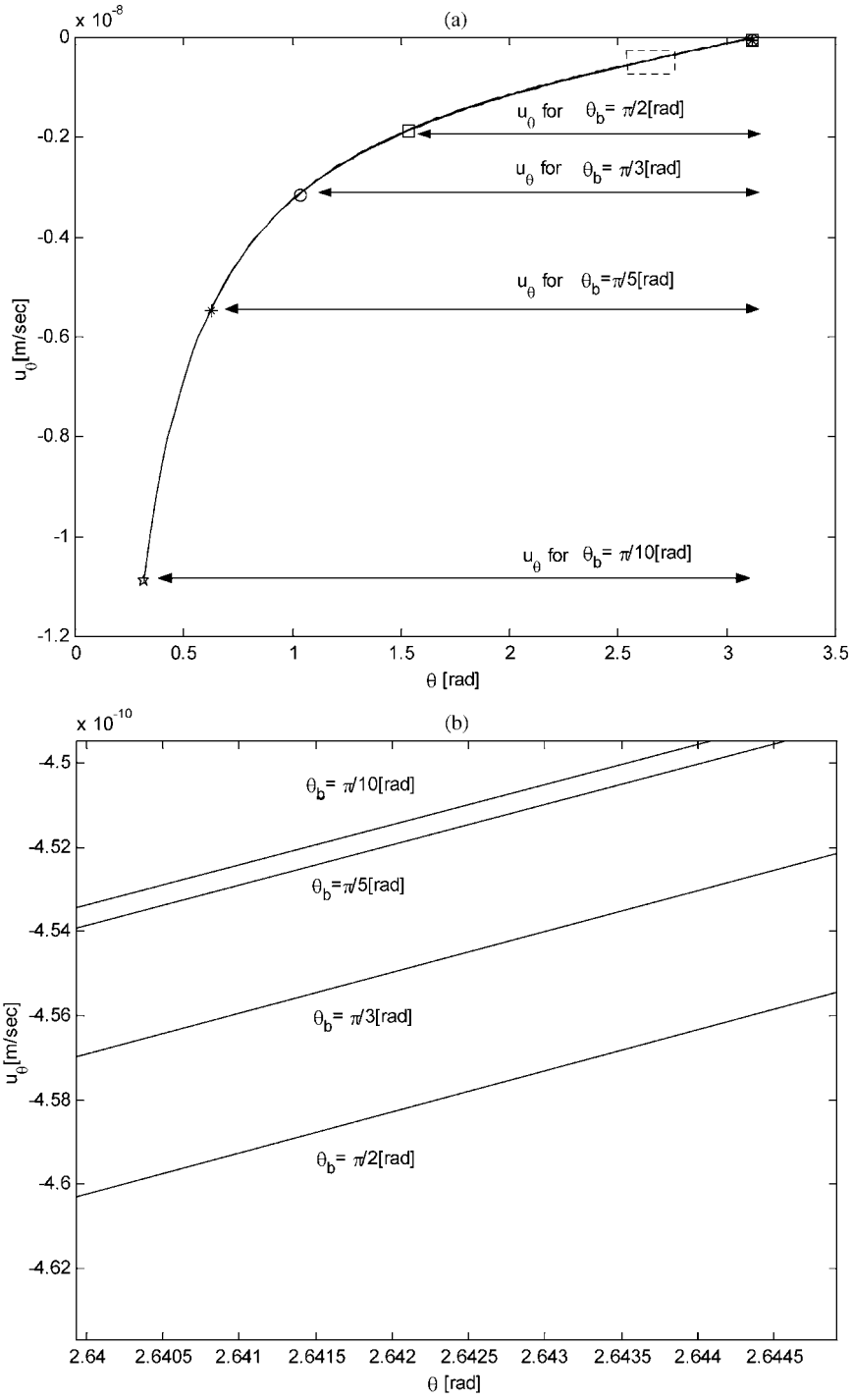

FIG. 12. (a) *The spatial distribution of the tangential velocity for various values of* θ_b. (b) *A blowup of the dotted small rectangle shown in* (a) *that manifests the small contribution of the angle* θ_b.

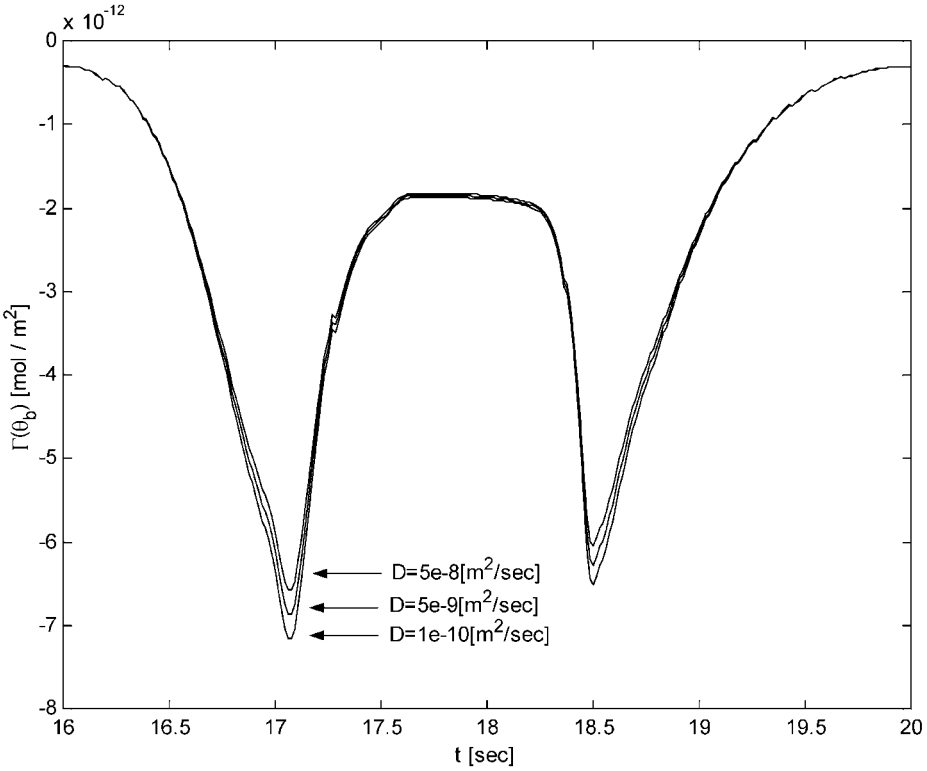

FIG. 13. *The temporal evolution of surfactant concentration* Γ *at* θ_b *for various values of the diffusion coefficient* D.

θ gets closer to θ_b. This result is consistent with the assumption that the fluid excess is generated uniformly at the alveolar surface.

The surfactant concentration and the tangential velocity dependence upon θ and θ_b are also illustrated in Figures 11 and 12, respectively. Figure 11 illustrates that $\gamma = \overline{\gamma} \overset{0}{\gamma} + \Gamma$ decreases and the surfactant concentration gradient increases as θ_b decreases. Hence, smaller values of θ_b yield a nonlinear increase in the magnitude of u_θ at the alveolar rim. This result is not surprising since, from (17h), if the Peclet number is large, u_θ varies like $\cot(\theta_b/2)$. Figure 12 illustrates how u_θ increases (in absolute value) as we approach the alveolar rim. It also illustrates that different values of θ_b result in almost identical values of u_θ, namely, all lines seem to collapse into a single graph within their mutual domain. However, a blowout of a small domain (shown by a small rectangle in the upper right corner of Figure 12) indicates that small deviations do exist between different values of θ_b (Figure 12(a)), with slightly smaller values of u_θ for smaller θ_b's.

The effect of the Peclet number upon surfactant distribution and the tangential velocity field is summarized in Figures 13–14. Figure 13 illustrates a double peaked pattern that results from the abrupt change in surface tension gradients at point A of Figure 2(b). Figure 14 illustrates dependence of u_θ upon time, with the highest (absolute) value occurring at the end of inhalation and the beginning of exhalation. Varying the diffusion coefficient has a minor effect on the results. This is not surprising since the Peclet number is quite high (Pe = 64) and the inverse of the capillary

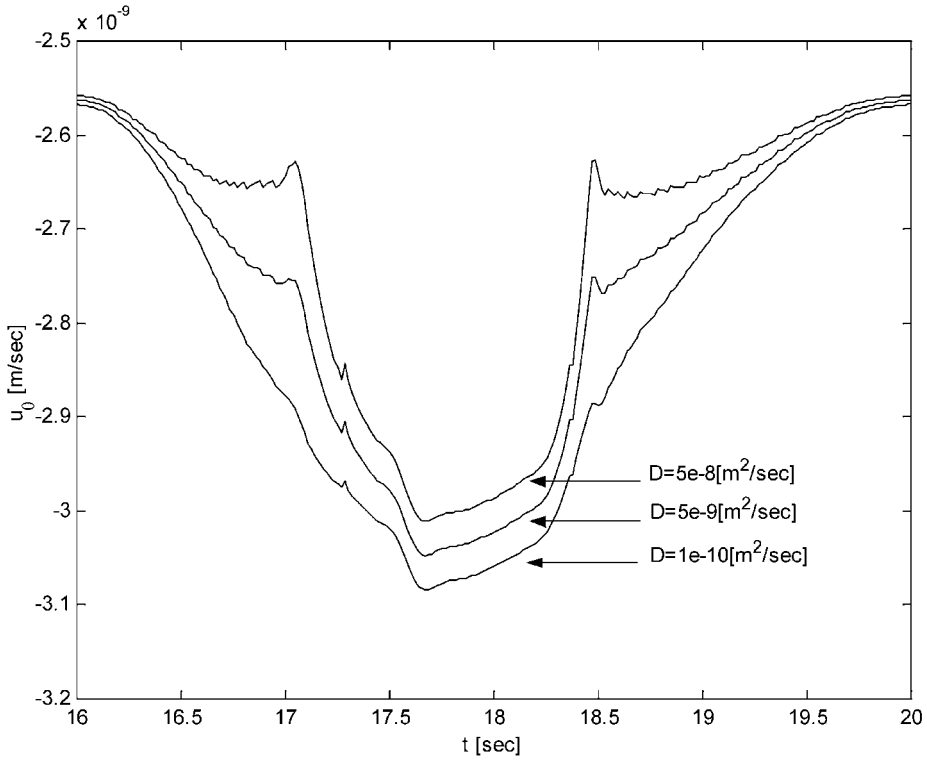

FIG. 14. *The temporal evolution of the tangential velocity U_θ at θ_b for various values of the diffusion coefficient D.*

number is about 16. A more significant effect would occur were D of the order of $D = 5 \times 10^{-8}$ m^2/sec, a much greater value than the estimated physical value of $D = 10^{-10}$ m^2/sec.

Finally, the surfactant production rate, λ_b, has a most significant effect on the tangential velocity. An increase in the production rate causes a concomitant increase in the tangential velocity.

7. Discussion and conclusions. The results in section 6 demonstrate that gradients in surfactant concentration at the lining layer interface induce tangential flow toward the alveolar edge (the Marangoni effect). Based upon experimental observations, we assumed that during every breathing cycle an excess amount of surfactant was secreted at the alveolus wall and removed to the adjacent airway. This excess amount is a given percentage of the existing average amount of surfactant that is embedded inside the lining layer. The removal of surfactants and the concomitant concentration gradients induce tangential flow inside the lining layer so that a small amount of the lining fluid exits the alveolus with a typical low rate on the order of 10^{-9} m/sec. The flow rate varies periodically with time and depends strongly upon how widely open the alveoli are. Pathologically wide cone angles θ_b result in a strong reduction in $\hat{U}_\theta$ and vice versa. However, since $u_\theta \sim \lambda_b \hat{U}_\theta$, the actual tangential velocity may either increase or decrease with θ_b. To make a rigorous conclusion, additional experimental evidence is required to correlate the flux of surfactant exiting the alveolus (proportional to λ_b) with the cone angle θ_b.

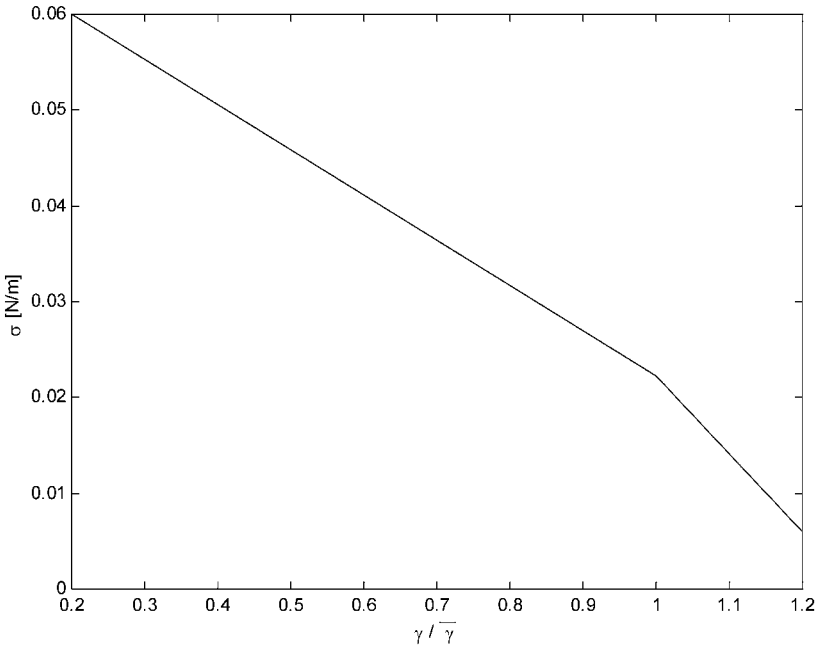

FIG. 15. *Surface tension dependency upon concentration of surfactant TA from Otis et al.* [19].

Particles that are deposited over the alveolus wall are subject to hydrodynamic drag and may be swept out of the alveolus due to the induced tangential velocity. The hydrodynamic cleansing rate is determined by particle velocity that, generally, need not be equal to the fluid velocity. However, the predicted fluid tangential velocity at the alveolar rim may provide a reasonable measure of the rate of hydrodynamic cleansing. With an average sweeping rate, it will take a particle about two days to move a distance equal to one alveolar radius, a very small rate indeed.

The effect of particle diffusion may add to the cleansing rate. However, this effect may be quite small. The diffusion coefficient of a particle 1μm in diameter in an *unbounded* lining flow field is $D_p = 3.8^{*}10^{-14}$ m^2/sec, based on the Stokes–Einstein equation. Thus, it seems that the time it takes a particle to travel a distance equal to one alveolar radius $R = 10^{-4}$m is of the order of $R^2/4D_p \sim 10^5$s, a value similar to the convection time. Notwithstanding this idea, Happel and Brenner [13] show that, due to the close proximity of the particle to the alveolar walls, the hydrodynamic drag coefficient can be several order of magnitudes higher than $6\pi\mu r_p$ (here r_p is the particle radius). Consequently, the value for the diffusion coefficient would be smaller and the resulting diffusion time longer.

We also tried to compare DPPC with an artificial surfactant TA (also known as Survanta; Ross Laboratories, Columbus, OH), widely used clinically to treat respiratory distress syndrome. From Otis et al. [19], a surfactant TA isotherm, relating the surface tension to surface concentration, is obtained (Figure 15) and approximated by two straight lines. Figures 16 and 17 illustrate the behavior of surfactant TA vis-à-vis DPPC, provided that their Peclet number is of similar order.[2] The time evolution of Γ differs markedly from that of DPPC; however, the calculated u_θ at θ_b is very similar.

[2]Note that synthetic surfactants do not undergo cellular secretion and adsorption. Thus, the results may depend on the time protocol by which TA is provided, but this is left for future work.

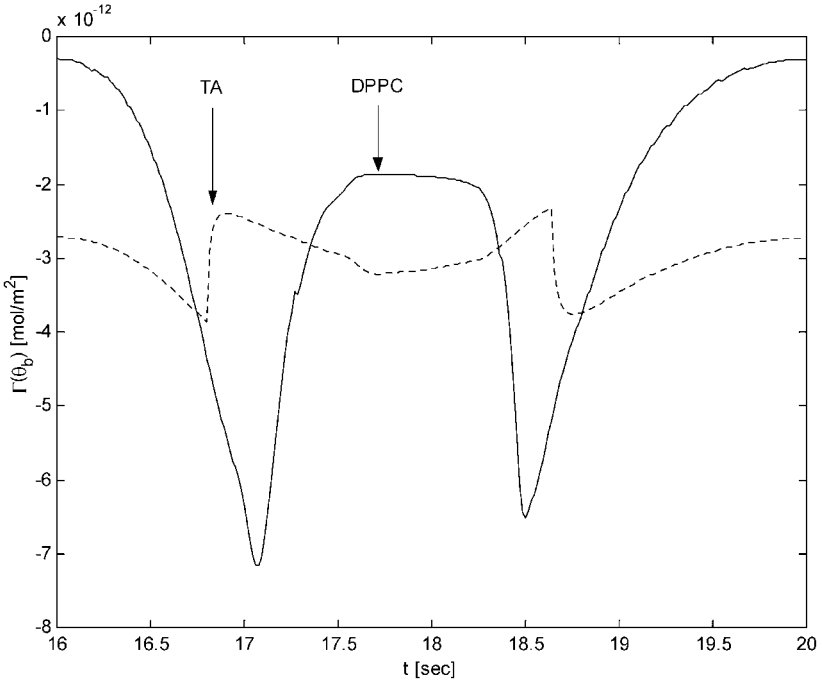

FIG. 16. *The temporal evolution of surfactant concentration* Γ *for DPPC and surfactant TA at* $\theta_b = \pi/3$.

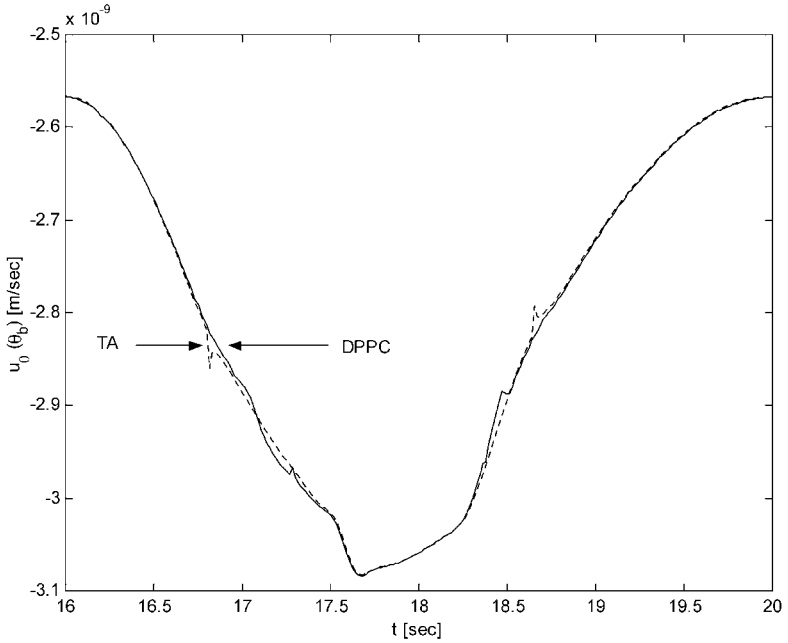

FIG. 17. *The temporal evolution of the tangential velocity for DPPC and surfactant TA at* $\theta_b = \pi/3$.

The small deviations stem from the discontinuity in $\partial\hat{\sigma}/\partial\hat{\gamma}$ assumed for surfactant TA. In fact, U_θ at θ_b should depend approximately linearly upon $\hat{R}$. Since, from (19a) and (19b), at $\hat{y} = 1/\hat{R}^2$ we obtain that

$$\hat{U}_\theta = \frac{\hat{W}}{\hat{R}^2} = \frac{\overline{C}_a^{-1}}{\hat{R}^3} \frac{\partial\hat{\sigma}}{\partial\hat{\gamma}}\bigg|_{\hat{\gamma}=1/\hat{R}^2} \frac{\partial\hat{\Gamma}}{\partial\theta},$$

consequently, at the alveolus edge $\theta = \theta_b$, for large Peclet numbers, boundary condition (21c) results in $\hat{U}_\theta|_{\theta=\theta_b} \sim -\hat{R}\cot(\theta_b/2)$. Thus, the major difference in the tangential velocity $u_\theta \sim \lambda_b \hat{U}_\theta$ between DPPC and surfactant TA stems from λ_b, provided that they possess similar diffusion coefficients.

In summary, a significant enhanced hydrodynamic cleansing can occur if the mechanism that keeps the surfactants from excessive accumulation or dilution functions over a wide range of surfactant concentrations. Notice that a very small deviation in surfactant concentration from the radially symmetric distribution is sufficient to induce flow in the lining layer. Thus, artificial stimulation of surfactant production at the alveolar wall tissue, or artificially administering a small excess amount of surfactant by inhalation, may result in an increased flow of surfactants exiting the alveoli and a concomitant sweeping flow of the lining layer. More research is required to investigate what the physiological mechanisms might be that cause surfactants to exit the alveolus and thereby determine/control the important parameter λ_b for various values of alveolus cone angle θ_b and surfactant composition. We hope that an artificial process can be devised and experimentally tested so that people exposed to a severe polluted environment could utilize the mechanism of enhanced hydrodynamic cleansing to reduce particle deposition of hazardous materials inside the lung alveoli.

Acknowledgments. The authors would like to thank Professor L. Gradon for his helpful explanations and Dr. A. Tsuda for illuminating discussions.

REFERENCES

[1] T. Ahmed, *Clinical testing of aerosol drugs*, in Respiratory Drug Delivery, P. R. Byron, ed., CRC Press, Boca Raton, FL, 1990, pp. 208–242.

[2] R. Ardila, T. Horie, and J. Hildebrandt, *Macroscopic isotropy of lung expansion*, Respir. Physiol., 20 (1974), pp. 105–115.

[3] R. Aris, *Vectors, Tensors, and the Basic Equations of Fluid Mechanics*, Prentice–Hall, Englewood Cliffs, NJ, 1962.

[4] P. Bezdicek and G. C. Crystal, *Pulmonary macrophages*, in The Lung: Scientific Foundations, 2nd ed., R. G. Crystal and J. B. West, eds., Lippincott-Raven, Philadelphia, 1997, pp. 859–874.

[5] J. Brain, J. D. Blanchard, and T. D. Sweeney, *Deposition and fate of inhaled pharmacological aerosol*, in Provocative Challenge Procedures: Background and Methodology, S. D. Spector, ed., Futura, Mount Kisco, NY, 1989, pp. 1–36.

[6] D. W. Dockery, J. D. Spengler, J. H. Ware, M. E. Fay, B. G. Ferris, and F. E. Speizer, *An association between air pollution and mortality in six U.S. cities*, N. Engl. J. Med., 329 (1993), pp. 1753–1759.

[7] J. Gil, H. Bachofen, P. Gehr, and E. R. Weibel, *Alveolar volume-surface area relation in air and saline filled lungs fixed by vascular perfusion*, J. Appl. Physiol., 45 (1979), pp. 990–1001.

[8] J. Gil and E. R. Weibel, *Morphological study of pressure-volume hysteresis in rat lungs fixed by vascular perfusion*, Respir. Physiol., 15 (1972), pp. 190–213.

[9] J. Goerke, *Pulmonary surfactant: Functions and molecular composition*, Biochim. Biophys. Acta, 1408 (1998), pp. 79–89.

[10] J. Goerke and J. A. Clements, *Alveolar surface tension and lung surfactant*, in Respiratory System, Vol. III, A. P. Fishman and S. R. Geiger, eds., Am. Physiol. Soc., Bethesda, MD, 1985, pp. 247–261.

[11] L. Gradon and A. Podgorski, *Hydrodynamical model of pulmonary clearance*, Chem. Eng. Sci., 44 (1989), pp. 741–749.

[12] S. Haber, J. P. Butler, H. Brenner, I. Emanuel, and A. Tsuda, *Shear flow over a self-similar expanding pulmonary alveolus during rhythmical breathing*, J. Fluid Mech., 405 (2000), pp. 243–268.

[13] J. Happel and H. Brenner, *Low Reynolds Number Hydrodynamics*, Prentice–Hall, Englewood Cliffs, NJ, 1965.

[14] B. G. Harvey and R. G. Crystal, *Pulmonary response to chronic inorganic dust exposure*, in The Lung: Scientific Foundations, 2nd ed., R. G. Crystal and J. B. West, eds., Lippincott-Raven, Philadelphia, 1997, pp. 2339–2352.

[15] S. Hawgood, *Surfactant: Composition, structure, and metabolism*, in The Lung: Scientific Foundations, 2nd ed., R. G. Crystal and J. B. West, eds., Lippincott-Raven, Philadelphia, 1997, pp. 557–571.

[16] J. Heyder, J. D. Blanchard, H. A. Feldman, and J. D. Brain, *Convective mixing in human respiratory tract: Estimates with aerosol boli*, J. Appl. Physiol., 64 (1988), pp. 1273–1278.

[17] T. J. R. Hughes, *The Finite Element Method, Linear, Static and Dynamic Finite Elements Analysis*, Prentice–Hall, Englewood Cliffs, NJ, 1987.

[18] A. Oron, S. H. Davis, and S. G. Bankoff, *Long-scale evolution of thin liquid films*, Rev. Modern Phys., 69 (1997), pp. 931–980.

[19] D. R. Otis, E. P. Ingenito, R. D. Kamm, and M. Johnson, *Dynamic surface tension of surfactant TA: Experiments and theory*, J. Appl. Physiol., 77 (1994), pp. 2681–2688.

[20] M. A. Sleigh, J. R. Blake, and N. Liron, *The propulsion of mucus by cilia*, Am. Rev. Respir. Dis., 137 (1988), pp. 726–741.

[21] M. C. Phillips and D. Chapman, *Monolayer characteristics of saturated* $1,2$*-diacyl phosphatidylcholines (lecitins) and phosphatidylethanolamines at the air-water interface*, Biochim. Biophys. Acta, 163 (1968), pp. 301–313.

[22] A. Podgorski and L. Gradon, *An improved mathematical model of hydrodynamical self-cleansing of pulmonary alveoli*, Ann. Occup. Hyg., 37 (1993), pp. 347–365.

[23] E. M. Scarpelli, *The Surfactant System of the Lung*, Lea & Febiger, Philadelphia, 1968.

[24] H. Schulz, P. Heilmann, A. Hillebrecht, J. Gebhart, M. Mayer, J. Piiper, and J. Heyder, *Convective and diffusive gas transport in canine intrapulmonary airways*, J. Appl. Physiol., 72 (1992), pp. 1557–1562.

[25] A. Tsuda, F. S. Henry, and J. P. Butler, *Chaotic mixing of alveolated fluid duct flow in rhythmically expanding pulmonary acinus*, J. Appl. Physiol., 79 (1995), pp. 1055–1063.

[26] A. Tsuda, Y. Otani, and J. P. Butler, *Acinar flow irreversibility caused by perturbations in reversible alveolar wall motion*, J. Appl. Physiol., 86 (1999), pp. 977–984.

[27] E. R. Weibel, *Functional morphology of lung parenchyma*, in Handbook of Physiology, The Respiratory System, Vol. 3, A. P. Fishman, ed., Am. Physiol. Soc., Bethesda, MD, 1986, pp. 89–111.

[28] A. de Wit, D. Gallez, and C. I. Christov, *Nonlinear evolution equations for thin films with insoluble surfactants*, Phys. Fluids, 6 (1994), pp. 3256–3266.

[29] T. B. Zeltner, T. D. Sweeney, W. A. Skornik, H. A. Feldman, and J. D. Brain, *Retention and clearance of* $0.9mm$ *particles inhaled by hamsters during rest or exercise*, J. Appl., Physiol., 70 (1991), pp. 1137–1156.